Chaos in the low-lying collective states of even-even nuclei: Quantal fluctuations

Y. Alhassid
Center for Theoretical Physics, Sloane Physics Laboratory, and A. W. Wright Nuclear Structure Laboratory, Yale University, New Haven, Connecticut 06511

A. Novoselsky
Racah Institute of Physics, The Hebrew University, Jerusalem, 91904, Israel
(Received 6 November 1991)

We study the fluctuations in the spectrum and the $E2$ transition intensities of the low-lying collective states in heavy nuclei. Using the interacting boson model we investigate the transition from rotational nuclei to γ-unstable nuclei. Near those two limits the system exhibits regular behavior but in the transition region we observe the onset of chaos where both the level statistics and the intensities statistics are described by the Gaussian orthogonal ensemble of random matrices. The systematics of the onset of chaos within different spin/parity classes are investigated. The quantal results agree with the classical mean-field analysis.

PACS number(s): 24.60.Lz, 21.60.Ev

I. INTRODUCTION

Random-matrix theories [1] (RMT's) were introduced to explain fluctuation properties of neutron and proton resonances in the compound nucleus [2,3]. Since the exact Hamiltonian of the heavy compound nucleus is not known, and due to its complexity and large number of degrees of freedom, it was natural to replace it by an ensemble of Hamiltonians. One then applies an ergodic hypothesis, where an average of a certain quantity over many nuclear states is replaced by a corresponding average over the ensemble. In RMT one assumes that all possible laws of interaction are equally probable, except that they must be consistent with the fundamental symmetries of the system. In particular, if the system has time-reversal symmetry, then the representation matrix of the Hamiltonian in a "real" basis is a real matrix. The Hamiltonian's matrices are, therefore, chosen to be real and symmetric. Since the probability density for a given Hamiltonian must be independent of the choice of the basis with respect to which it is represented, this probability measure should be invariant under orthogonal transformations. We are then led to the Gaussian orthogonal ensemble (GOE), whose fluctuation properties were used to explain the neutron resonances and their widths.

In recent years, however, a new understanding of the use of random matrices has emerged. It was conjectured that their validity can be extended to analyze spectral fluctuations in quantal system with small number of degrees of freedom (even two), when the corresponding classical motion is completely chaotic. This conjecture was put forward by Bohigas, Giannoni, and Schmit [4], based on the quantal analysis of the Sinai's billiard which was known to be classically chaotic. It was then confirmed by numerous studies of systems in two degrees of freedom [5-10]. Semiclassical arguments were used by Berry [11] to show that the two-level cluster correlation function of a classically chaotic system agrees with the predictions of the Gaussian orthogonal ensemble (GOE). It was further shown in several model studies of classically chaotic systems that the fluctuations of the matrix elements of a generic transition operator are consistent with the GOE analysis [12–14].

Experimentally, the most complete data available is the nuclear data ensemble (NDE) consisting of 1762 neutron and proton resonance energies corresponding to 36 sequences in 32 different nuclei [15]. These resonances are in the region of high nuclear level density, and they show a remarkable agreement with GOE. The question that then arises naturally, with the new understanding of the applicability of RMT, is whether chaos could also prevail in the low-lying collective part of the nuclear spectrum. A similar question was raised by Abul-Magd and Weidenmuller [16] through the analysis of experimentally known low-lying levels in nuclei. However, to obtain a reasonable statistic it was necessary to group together levels of different nuclei and of different spin/parity. The conclusions reached were, therefore, only partial. More recently, an attempt was done to extract the dependence of the statistical fluctuations of the spectrum on the nuclear species [17]. Also here it was necessary to take levels from a wide range of energies and angular momenta. Raman *et al.* [18] investigated a complete set of experimental levels in ^{116}Sn, and Garrett *et al.* [19] analyzed a large number of low-lying near yrast states from nuclei in the region $A=155-185$.

The purpose of this paper is to study the chaotic properties of the low-lying collective states of even-even nuclei by using a realistic theoretical model [20]. It is important to note that most studies of quantum chaos were restricted to unrealistic models in two degrees of freedom. The only exception is that of the hydrogen atom in strong magnetic fields [21]. A realistic description of the low-lying part of the nuclear spectra requires a model with at least five degrees of freedom, corresponding to the nu-

clear quadrupole deformation. This larger number of degrees of freedom make the study of quantum and classical chaos in a realistic nuclear model a much more challenging project. Furthermore, there is also a general theoretical interest in studying such systems, showing that the connection between the eigenvalue and eigenvector statistics holds even for systems with more than two degrees of freedom.

The model that we use is the interacting boson model [22,23] which describes well the low-energy part of the nuclear spectrum for a large volume of heavy nuclei. In particular, we investigate the transition between rotational nuclei and γ-unstable nuclei. The classical mean-field limit of the model was discussed in detail in Ref. [24]. Here we shall do the quantal analysis. While most studies of quantum chaos are restricted to the study of spectral fluctuations alone, we shall study in addition the fluctuations of the matrix elements. In particular we shall study the distributions of the $E2$ intensities [10]. We find that the quantal results generally agree with the classical analysis, and we observe the onset of quantum chaos in the intermediate region between rotational and γ unstable nuclei. There are, however, important effects which are purely quantal and do not have a classical counterpart.

The outline of the paper is as follows. In Sec. II we introduce the quantal model that is used in our study. As an algebraic model it has several advantages, and in particular the completely integrable limits can be related to the dynamical symmetry limits of the model [20,25]. In Sec. III we discuss the spectral statistics and in Sec. IV the transition intensity fluctuations and in particular the $B(E2)$ distributions are analyzed. More detailed results and systematics are discussed in Sec. V where the level and $E2$ statistics are shown for various spin/parity classes.

II. THE QUANTUM MODEL

A. Hamiltonian and transition operator

The algebraic model that we use to describe the low-lying collective states in nuclei is the interacting boson model (IBM). When no distinction is made between protons and neutrons (IBM-1), the model degrees of freedom are an s boson with spin/parity 0^+ and five quadrupole d bosons with spin/parity 2^+. In the self-consistent Q formalism the Hamiltonian [26] has the form

$$H=c_0 n_d+c_1\mathbf{L}^2+c_2 Q^\chi\cdot Q^\chi \ . \tag{1}$$

In Eq. (1), c_0, c_1, and c_2 are parameters, while n_d, $\mathbf{L}$, and Q^χ are the number of d bosons, the angular momentum, and the quadrupole operator, respectively,

$$n_d=d^\dagger\cdot\tilde{d} \ , \tag{2a}$$

$$\mathbf{L}=\sqrt{10}(d^\dagger\times\tilde{d})^{(1)} \ , \tag{2b}$$

$$Q^\chi=(d^\dagger\times s+s^\dagger\times\tilde{d})^{(2)}+\chi(d^\dagger\times\tilde{d})^{(2)} \ . \tag{2c}$$

We have used the operators $\tilde{d}_\mu$,

$$\tilde{d}_\mu=(-)^\mu d_{-\mu} \ , \tag{3}$$

which transform under rotation like $d^\dagger_\mu$.

The quadrupole operator depends on a parameter χ which usually varies in the range $-\sqrt{7}/2\le\chi\le 0$. Electromagnetic transition operators can also be constructed within the framework of the model. In this paper we shall use in particular the $E2$ operator, which in the self-consistent Q formalism is proportional to Q^χ

$$T(E2)=\alpha_2 Q^\chi \ . \tag{4}$$

The $B(E2)$ intensity for a transition from state i to state f is given in terms of the reduced matrix element of $T(E2)$:

$$B(E2;i\to f)=\frac{1}{2J_i+1}|\langle f\|T(E2)\|i\rangle|^2 \ . \tag{5}$$

The statistical fluctuations of the $B(E2)$ intensities will play an important role in the understanding of the onset of chaos in nuclei.

In the present paper we shall investigate the family of Hamiltonians (1) for $c_0=0$ and $-\sqrt{7}/2\le\chi\le 0$.

B. Algebraic structure

The 36 generators $\{b_i^\dagger b_j\}$, where $\{b_i^\dagger\}=\{s^\dagger,d_\mu^\dagger(\mu=-2,\ldots,2)\}$, span an algebra $G=\mathrm{U}(6)$. The Hilbert space of the physical states carries a representation of the U(6) algebra [23], and the Hamiltonian is a quadratic function of the generators of U(6).

An algebraic model has several advantages over more conventional models in the analysis of chaos. The first is that the number of bound states is finite since the unitary representations of any compact group G are finite dimensional. It is, therefore, possible to diagonalize the Hamiltonian with no truncation errors. This is useful because in the statistical analysis it is important to get an accurate and complete set of eigenvalues. Any model of low-lying collective states of nuclei will have at least five degrees of freedom, corresponding to the five nuclear quadrupole degrees of freedom. To solve accurately a Schrödinger equation for that number of degrees of freedom and a large number of eigenvalues is a formidable task. Already the problem of the hydrogen atom in a strong magnetic field, which has only two degrees of freedom was quite difficult to solve numerically [21].

Another important advantage of an algebraic model is that completely integrable Hamiltonians whose associated motion is regular can be easily identified. They are related to dynamical symmetries. A dynamical symmetry [27] in an algebraic model described by an algebra G occurs when the Hamiltonian is of the form

$$H=\alpha_0 C(G)+\alpha_1 C(G^{(1)})+\alpha_2 C(G^{(2)})+\cdots \ , \tag{6}$$

where

$$G=G^{(0)}\supset G^{(1)}\supset G^{(2)}\supset\cdots \tag{7}$$

is a chain of subalgebras of G and each $C(G^{(i)})$ is a Casimir invariant of the corresponding algebra $G^{(i)}$. The Hilbert space carries a representation of G, whose basis states can be labeled by the eigenvalues of the above Casimir invariants. These states are eigenstates of (6) and

the corresponding energies are found by substituting in (6) the eigenvalues of the Casimir invariants.

The IBM-1 has three dynamical symmetries [23]

$$U(6)\supset \left\{ \begin{matrix} U(5)\supset O(5) \\ SU(3) \\ O(6)\supset O(5) \end{matrix} \right\} \supset O(3) \quad \begin{matrix} (I) \\ (II) \\ (III) \end{matrix} , \tag{8}$$

which describes vibrational nuclei [chain (I)], rotational nuclei [chain (II)], and γ-unstable nuclei [chain (III)]. In the self-consistent Q formalism they occur as follows: Chain (I) is obtained for $c_2=0$, since n_d is a linear Casimir invariant of U(5). Chain (II) is obtained for $c_0=0$, $\chi=-\sqrt{7}/2$ since $Q^\chi\cdot Q^\chi$ is then related to the quadratic Casimir invariant of SU(3). Finally, chain (III) occurs for $c_0=0$, $\chi=0$ since the respective $Q^\chi\cdot Q^\chi$ is then a combination of the quadratic Casimir invariants of O(6) and O(5)

$$Q^\chi\cdot Q^\chi|_{\chi=0}=C_2(O(6))-C_2(O(5)) . \tag{9}$$

To see how a dynamical symmetry is related to complete integrability, notice that the set of Casimir invariants

$$\{C(G),C(G^{(1)}),C(G^{(2)}),\ldots\} , \tag{10}$$

form a set of constants of the motion of H in (6), which are in involution

$$[H,C(G^{(i)})]=0 , \tag{11}$$

$$[C(G^{(i)}),C(G^{(j)})]=0 . \tag{12}$$

To have a completely integrable system we need a complete set of constants in involution, i.e., their number should be equal to the number of degrees of freedom. If the above set (10) is not complete, there is a missing label in one or more of the reductions $G^{(i)}\supset G^{(i+1)}$. It is then possible [28] to find an invariant of $G^{(i+1)}$ that is built from the generators of $G^{(i)}$ and is not a Casimir invariant of $G^{(i)}$. Such invariants commute with all the Casimir operators in (10), and by adding them to (10), we get a complete set of constants of the motion.

III. SPECTRAL FLUCTUATIONS

A. Density of states

To analyze the statistical fluctuations of the spectrum $\{E_i\}$, it is necessary, as usual, to separate its smoothed average part whose behavior is nonuniversal and cannot be described by random-matrix theory [29] (RMT). To do so we construct the staircase function of the spectrum $N(E)$, defined as the number of levels below E and separate it into average and fluctuating parts

$$N(E)=N_{\rm av}(E)+N_{\rm fluct}(E) . \tag{13}$$

The nonuniversal part $N_{\rm av}(E)$ may be found semiclassically. Here we have taken it to be the fit of a smooth function to the staircase $N(E)$. We have tried two classes of fitting functions: Polynomials of degree M in E and cubic splines [30]. Among the polynomial class we found that $M=6$ is best. Figure 1 shows (left column) such a typical polynomial fit to the staircase function $N(E)$ as well as a cubic spline fit. The statistical fluctuations of the spectrum are found to be quite independent of the fitting class. In the following we shall use polynomial fits with $M=6$. The unfolded spectrum is defined by the mapping

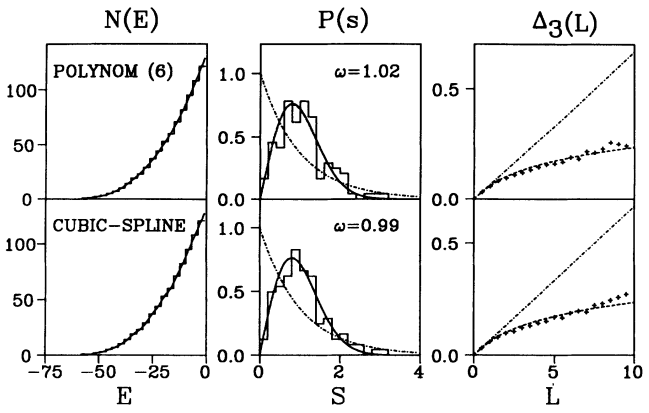

FIG. 1. Comparison of spectral fluctuations for two different classes of fitting functions to the staircase function $N(E)$: a polynomial of sixth order (top row) and a cubic-spline fit (bottom row). The levels analyzed are the $J=8^+$ levels of the Hamiltonian (1) with $c_0=0$, $\chi=-0.6$, and $N=20$ bosons. Left column: the staircase function $N(E)$ and the fit $N_{\rm av}(E)$ (solid line). Middle column: the level spacing distribution $P(S)$ and the fit with a Brody distribution (18) (solid lines) with the quoted ω. Right column: the Dyson-Metha statistics $\Delta_3(L)$ described by the + symbols. The dashed lines are the GOE limit and the dash-dotted lines are the Poisson statistics.

$$\tilde{E}_i=N(E_i) . \tag{14}$$

The unfolded levels $\tilde{E}_i$ have a constant average spacing, but the actual spacings show strong fluctuations.

We note that when good quantum numbers are known, it is important to analyze separately states that belong to different quantum numbers. In our studies spin and parity (J^π) are good quantum numbers so we analyze levels separately within each spin/parity class.

B. Level spacing distribution

We have used two statistical measures to determine the fluctuation properties of the unfolded levels: the nearest-neighbor level spacing distribution $P(S)$ and the Δ_3 statistics of Dyson and Metha. The level spacing distribution is defined as the probability of two neighboring levels to be a distance S apart. A regular system is expected to behave by the Poisson statistics where the eigenvalues are uncorrelated and

$$P(S)=e^{-S} . \tag{15}$$

If the system is classically chaotic, we expect to obtain the Wigner distribution

$$P(S)=(\pi/2)S\exp(-\pi S^2/4) , \tag{16}$$

which is consistent with the GOE statistics [1–3]. We

have calculated the spacings S_i from the unfolded spectrum

$$S_i=\tilde{E}_{i+1}-\tilde{E}_i \tag{17}$$

and histogrammed them. An example is shown in the middle column of Fig. 1 for the $J=8^+$ levels of the Hamiltonian (1) with $N=20$ bosons, $c_0=0$, and $\chi=-0.6$. The dash-dotted line is the Poisson distribution (15), and the dashed line is the Wigner distribution (16). In the case shown the actual histogram is very close to the Wigner distribution. We have fitted the level spacing distribution to a Brody distribution (solid lines in Fig. 1) of the form

$$P_\omega(S)=AS^\omega\exp(-\alpha S^{1+\omega}) , \tag{18}$$

where

$$\alpha=\Gamma[(2+\omega)/(1+\omega)]^{1/2}$$

and

$$A=(1+\omega)\alpha \tag{19}$$

are chosen such that P is normalized to 1 and $\langle S\rangle=1$. The Brody distribution interpolates between the Poisson distribution ($\omega=0$) and the Wigner distribution ($\omega=1$).

C. Δ_3 statistics

The Δ_3 statistics was introduced by Dyson and Metha to measure the "rigidity" of the spectrum. It is defined by

$$\Delta_3(\alpha,L)=\min_{A,B}\frac{1}{L}\int_\alpha^{\alpha+L}[N(\tilde{E})-(A\tilde{E}+B)]^2d\tilde{E} \tag{20}$$

and measures the deviation of the staircase function (of the unfolded spectrum) from a straight line. A rigid spectrum corresponds to smaller values of Δ_3, while a soft spectrum has a larger Δ_3. In order to obtain a smoother function $\bar{\Delta}_3(L)$, we average $\Delta_3(\alpha,L)$ over several n_α intervals $(\alpha,\alpha+L)$

$$\bar{\Delta}_3(L)=\frac{1}{n_\alpha}\sum_\alpha\Delta_3(\alpha,L) . \tag{21}$$

The successive intervals are taken to overlap by $L/2$. A useful formula to calculate $\Delta_3(\alpha,L)$ was derived by Bohigas and Giannoni [29] in terms the ordered eigenvalues $\tilde{E}_1,\tilde{E}_2,\ldots,\tilde{E}_n$ in the interval $(\alpha,\alpha+L)$. Measuring $\tilde{E}_i$ with respect to the center of the interval $\epsilon_i=\tilde{E}_i-(\alpha+L/2)$ we have

$$\Delta_3(\alpha,L)=\frac{n^2}{16}-\frac{1}{L^2}\left[\sum_{i=1}^n\epsilon_i\right]^2+\frac{3n}{2L^2}\left[\sum_{i=1}^n\epsilon_i^2\right]-\frac{3}{L^4}\left[\sum_{i=1}^n\epsilon_i^2\right]^2+\frac{1}{L}\left[\sum_{i=1}^n(n-2i+1)\epsilon_i\right] . \tag{22}$$

The Δ_3 statistics is related to the two-level correlation function. The number statistics $n(L)$ is defined to be the number of levels in an energy interval of length L. Since the spectrum was unfolded, the average number statistics $\langle n(L)\rangle=L$ is independent of the spectrum. However, the variance of $n(L)$

$$\Sigma^2(L)=\langle[n(L)-\langle n(L)\rangle]^2\rangle \tag{23}$$

does depend on the spectrum considered. For the Poisson statistics,

$$\Sigma^2(L)=L , \tag{24}$$

while for the GOE

$$\Sigma^2(L)=\frac{2}{\pi^2}\left[\ln(2\pi L)+\gamma+1+\tfrac{1}{2}[\mathrm{Si}(\pi L)]^2-\frac{\pi}{2}\mathrm{Si}(\pi L)-\cos(2\pi L)-\mathrm{Ci}(2\pi L)+\pi^2L\left[1-\frac{2}{\pi}\mathrm{Si}(2\pi L)\right]\right] . \tag{25}$$

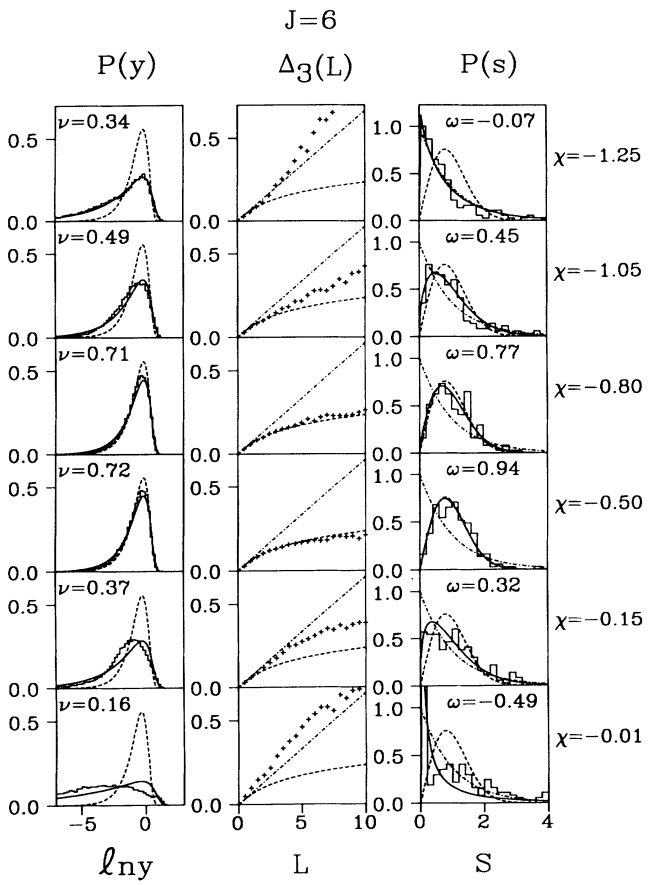

FIG. 2. Spectral and intensity fluctuations for the $J=6^+$ levels of the Hamiltonian (1) with $N=25$ bosons and various χ values between the rotational ($\chi=-\sqrt{7}/2$) and γ-unstable ($\chi=0$) limits ($c_0=0$). Right column: the level spacing distribution $P(S)$ where the solid line is the best-fitted Brody distribution with the quoted ω. Middle column: the Δ_3 statistics of Dyson and Metha denoted by the + symbols. Left column: the $E2$ intensity distribution $P(y)$ where the solid lines are χ^2 distributions in ν degrees of freedom (41) with the quoted ν. In all columns dashed lines describe the GOE statistics and dash-dotted lines the Poisson statistics.

Here γ is the Euler constant and Si, Ci are the sine and cosine integrals, respectively. The Δ_3 statistics can be calculated from the variance of the number statistics by

$$\bar{\Delta}_3(L)=\frac{2}{L^4}\int_0^L (L^3-2L^2r+r^3)\Sigma^2(r)dr \ . \tag{26}$$

For the Poisson statistics

$$\bar{\Delta}_3(L)=\frac{L}{15} \ , \tag{27}$$

while the asymptotic result for the GOE is

$$\bar{\Delta}_3(L) \underset{L\gg 1}{\approx} \frac{1}{\pi^2}\ln L-0.007 \ . \tag{28}$$

The GOE spectrum exhibits long-range order as is demonstrated by its low $\bar{\Delta}_3$ values as compared with the Poisson statistics.

The Δ_3 statistics calculated from (22) and (21) is demonstrated on Fig. 1 (right column) and is denoted by the + symbols. The Poisson limit is the dash-dotted line, and the GOE Δ_3 statistics is the dashed line. The actual case shown is very close to the GOE limit, and this result is consistent with the level spacing distribution.

D. Spectral fluctuations versus χ

We have analyzed the level statistics within each spin/parity class for the Hamiltonian (1) using $N=25$ bosons and $c_0=0$. The large number of bosons is chosen to obtain better statistics. Figure 2 shows a typical example for the $J=6^+$ levels for which the statistics is studied versus the parameter χ. The level spacing distribution $P(S)$ (right column) and the $\Delta_3(L)$ Dyson-Metha statistics (middle column) are shown for $\chi=-1.25$, -1.05, -0.8, -0.5, -0.15, and -0.01. Near the two dynamical symmetry limits ($\chi=-\sqrt{7}/2$ and $\chi=0$) we obtain a behavior close to Poisson as is expected for a completely integrable system. However, as χ changes away from these two limits we observe that the statistics is gradually changing to the GOE. This indicates the onset of chaos and is consistent with the results of the mean-field "classical" limit $N\to\infty$ discussed in Ref. [23]. In the range $-0.8\lesssim\chi\lesssim-0.4$ the system is mostly chaotic.

We note that when χ is very close to one of the dynamical symmetry limits (e.g., $\chi=-0.01$) we obtain negative values of ω, and the values of Δ_3 are even larger than the Poisson limit. This is a result of degeneracies that may occur in a dynamical symmetry limit and are related to missing labels. For instance, in the SU(3) limit of rotational nuclei, the K quantum number is a missing label in the reduction from SU(3) to O(3). Since K is not associated with a Casimir invariant, the energy eigenvalues in the SU(3) dynamical symmetry limit are independent of K. In the O(6) limit of γ-unstable nuclei, there is also such a missing label [23] in the reduction from O(5) to O(3), which is denoted by ν_Δ.

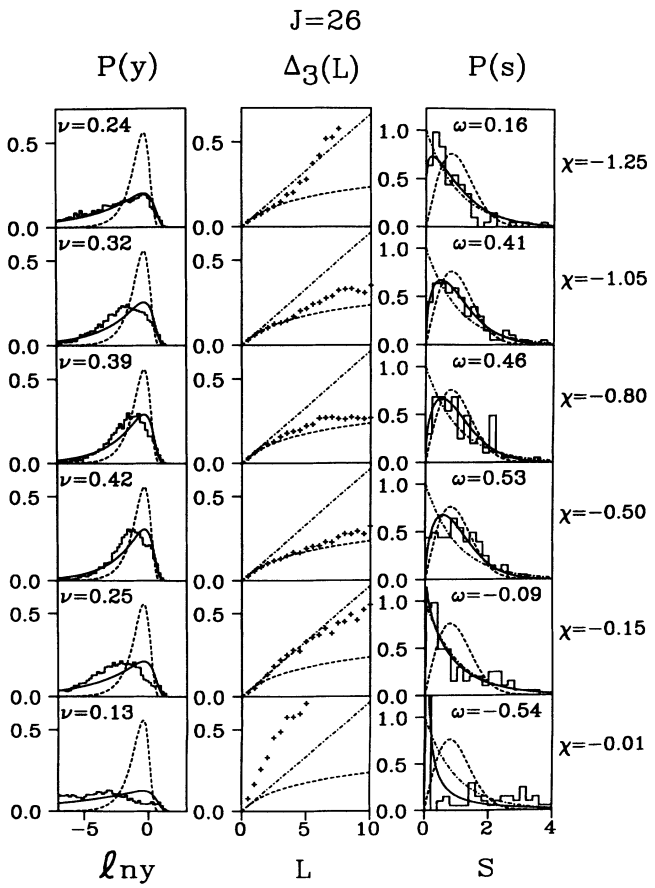

FIG. 3. As in Fig. 2 but for $J=26^+$.

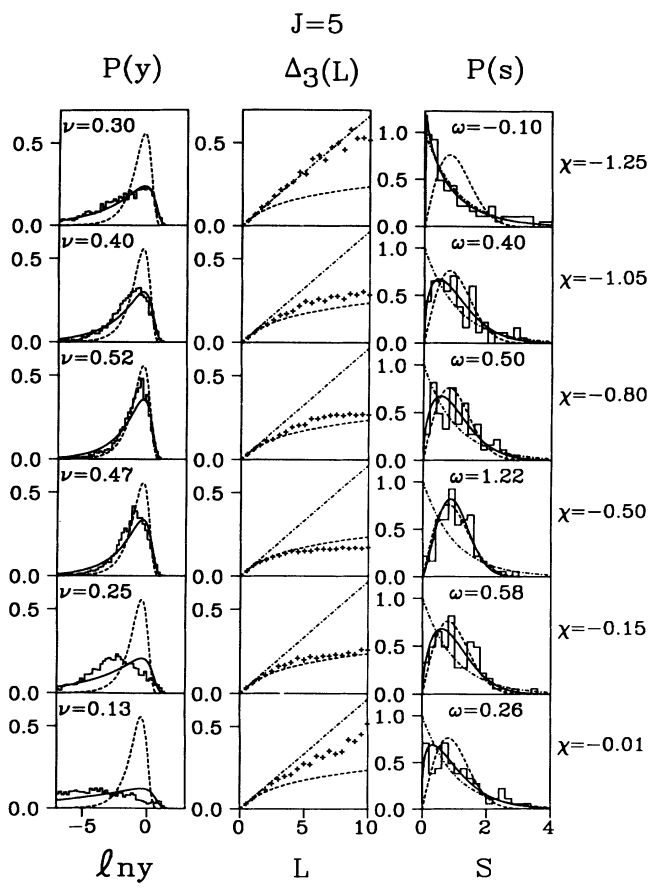

FIG. 4. As in Fig. 2 but for $J=5^+$.

It is interesting to observe the spin dependence of the statistics at a given χ. An example of high spin ($J=26^+$) is given in Fig. 3, and an example of odd spin ($J=5^+$) is given in Fig. 4. At low spins ($J \lesssim 10\hbar$) the statistics does not change much with J, except that near the O(6) limit ($-0.15 \lesssim \chi \leq 0$) we observe more regularity with increasing J. At high spins, however, we see a significant decrease of chaoticity as the spin increases. For example, at $\chi=-0.8$, ω drops from a value of $\omega=0.96$ at $J=10\hbar$ to a value of $\omega=0.46$ at $J=26\hbar$ (see Fig. 3). In fact the region $-0.8 \lesssim \chi \lesssim -0.4$, which is almost fully chaotic at low spins ($J \lesssim 16\hbar$), becomes intermediate between the regular and chaotic statistics at high spins. This behavior correlates nicely with the classical results; see in particular Fig. 9 of Ref. [24].

IV. INTENSITY FLUCTUATIONS

Matrix elements of transition operators probe the system's wave functions so that their statistical fluctuations provide additional information. It was shown that for a classically chaotic system, the matrix elements of a generic time-reversal-invariant operator should have the GOE fluctuation properties [13,14].

A. Intensity distribution

To find the distribution of matrix elements in the GOE, note that the distribution of the components a_i of a fixed vector $|\alpha\rangle$ along the random Hamiltonian eigenstates is given by [3]

$$P(a_1,a_2,\ldots) \propto \delta\left[\sum_i a_i^2 - 1\right] . \tag{29}$$

Denoting the value of a specific matrix element, say, a_1, by x we obtain its distribution $P^0(x)$ from

$$P^0(x)=\int P(a_1=x,a_2,\ldots)da_2 \cdots . \tag{30}$$

The result is

$$P^0(x)=\frac{1}{\sqrt{\pi}}\frac{N-1}{N}\frac{\Gamma(N/2+1)}{\Gamma(N/2+\frac{1}{2})}(1-x^2)^{(N-3)/2} , \tag{31}$$

which in the limit of large N can be written as

$$P^0(x) \approx (2\pi\langle x^2\rangle)^{-1/2} e^{-x^2/2\langle x^2\rangle} . \tag{32}$$

The distribution of intensities $y=x^2$ is then given by the Porter-Thomas distribution [31]

$$P^0(y)=(2\pi\langle y\rangle)^{-1/2} y^{-1/2} \exp(-y/2\langle y\rangle) . \tag{33}$$

For any operator T, we can define the transition intensities

$$y=|\langle f|T|i\rangle|^2 , \tag{34}$$

and construct their distribution $P(y)$ to be such that $P(y)dy$ is the probability of finding an intensity in the interval dy around y. To find this distribution in the GOE limit, we define the normalized vector $|\alpha\rangle$ by

$$|\alpha\rangle = T|i\rangle / \langle i|T^\dagger T|i\rangle . \tag{35}$$

The distribution $P(x)$ of Eq. (32) provides, then, the distribution of the matrix elements $\langle f|T|i\rangle$, while the distribution $P(y)$ given in (33) is the transition intensities distribution.

An alternative derivation of the Porter-Thomas distribution is through the principle of maximal entropy [13]. It has a conceptual and practical advantage since it is derived not for an ensemble of Hamiltonians. For a given state $|i\rangle$, the intensities satisfy a sum rule

$$\sum_f |\langle f|T|i\rangle|^2 = \langle i|T^\dagger T|i\rangle . \tag{36}$$

Rewriting (36) in terms of the amplitude distribution $P(x)$ we have

$$\int x^2 P(x)dx = \frac{1}{N}\langle i|T^\dagger T|i\rangle , \tag{37}$$

where N is the total number of states. The sum rule (37) always holds irrespective of the nature of the system's dynamics. To choose a distribution that is least biased among all distributions $P(x)$, which satisfy (37), we maximize the entropy

$$S[P]=-\int P(x)\ln P(x)dx . \tag{38}$$

We find a distribution $P^0(x)$ of the form (32) with

$$\langle x^2\rangle = \frac{1}{N}\langle i|T^\dagger T|i\rangle . \tag{39}$$

Since the intensity $y=x^2$, we have $P(y)=2P(x)(dx/dy)$ and using Eq. (32) we obtain for $P^0(y)$ the Porter-Thomas distribution (33). Thus we may interpret the Porter-Thomas distribution as the one that maximizes the entropy when no constraints are imposed, except for the ever present sum rule (36).

$P^0(x)$ is the expected distribution in the chaotic limit. In general, however, the distribution (32) need not agree with the data. We can then use (32) as a reference distribution. The deviation of a distribution $P(x)$ [that satisfies the constraint (37)] from $P^0(x)$ can be measured by the difference I of their entropies

$$I=S[P^0]-S[P]=\int P(x)\ln\left[\frac{P(x)}{P^0(x)}\right]dx , \tag{40}$$

where we have used $\int P(x)\ln P^0(x)=\int P^0(x)\ln P^0(x)dx$ [which follows from the fact that both $P(x)$ and $P^0(x)$ satisfy the same constraint $\langle x^2\rangle$]. The quantity I is also known as the information content [32] of P relative to P^0. It is always positive except when $P=P^0$, where $I=0$.

When a dynamical system is making a transition from chaotic to regular motion, we expect to find deviations from $P^0(x)$. To describe such deviations quantitatively we have introduced the χ^2 distribution in ν degrees of freedom [13]

$$P_\nu(y)=Ay^{\nu/2-1}\exp(-\nu y/2\langle y\rangle) , \tag{41}$$

where

$$A=\frac{(\nu/2\langle y\rangle)^{\nu/2}}{\Gamma(\nu/2)} . \tag{42}$$

The Porter-Thomas distribution is obtained for $\nu=1$. We have found [14] that the generic situation is that as a chaotic system becomes classically more regular, the

value of ν decreases monotonically from 1 towards 0. The reason is that as the system is approaching a regular behavior, selection rules become operative. Few transitions are quite strong, while many others are very weak.

It is possible to derive the distribution (41) by imposing the constraint

$$\langle \ln y \rangle = \int dy \ln y \, P(y) , \tag{43}$$

in addition to (37). Maximizing the entropy with the two constraints (37) and (43) we obtain the distribution (41). The value of the constraint for the distribution $P_\nu(y)$ is

$$\langle \ln(y/\langle y \rangle) \rangle = \psi(\nu/2) - \ln(\nu/2) , \tag{44}$$

where $\psi(z) = d \ln\Gamma(z)/dz$ is the psi function. The Langrange multiplier conjugate to the constraint (44) is $(\nu-1)/2$ and vanishes for the Porter-Thomas distribution $\nu=1$. The quantity (44) is plotted versus ν in Fig. 5.

As ν decreases, the distribution (41) becomes wider for a fixed $\langle y \rangle$. This can be seen from the expression for the variance of y

$$\langle (y - \langle y \rangle)^2 \rangle = 2\langle y \rangle^2/\nu . \tag{45}$$

Figure 6 shows several χ^2 distributions in ν degrees of freedom for $\nu=1$, 0.5, and 0.2, which have the same $\langle y \rangle$. To exhibit the important region of weak intensities y, we have plotted the distribution $P_\nu(\ln y)$, which is given by

$$P_\nu(\ln y) \propto y^{\nu/2} \exp(-\nu y/\langle y \rangle) . \tag{46}$$

To find ν for a given intensity distribution $P(y)$, we can minimize the information content of P relative to P_ν

$$I = \int P(y) \ln \left[\frac{P(y)}{P_\nu(y)} \right] dy . \tag{47}$$

In practice, we find $P(y)$ by histogramming the calculated intensities into a certain number of bins. The integral (47) can then be expressed as a discrete sum. It can be shown [33] that the condition of minimizing I in Eq. (47) with respect to ν is that the two constraints $\langle y \rangle$ and $\langle \ln y \rangle$, calculated with $P_\nu(y)$ are equal to those calculated with $P(y)$. An operational way to calculate ν is then to determine $\langle y \rangle$ and $\langle \ln(y/\langle y \rangle) \rangle$ from the known distribution $P(y)$. We find ν by inverting Eq. (44).

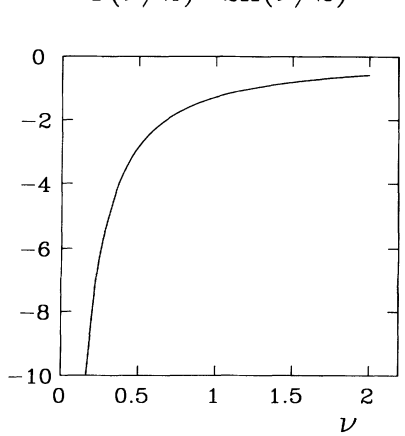

FIG. 5. The second constraint $\ln(y/\langle y \rangle)$ vs ν [Eq. (44)].

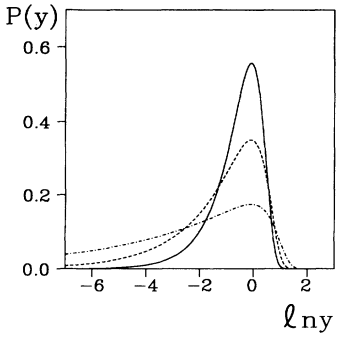

FIG. 6. The χ^2 distribution in ν degrees of freedom P_ν plotted vs $\ln y$ for $\nu=1$ (solid line), 0.5 (dashed line), and 0.2 (dash-dotted line).

B. Secular variations with energy

The fluctuation properties discussed in Sec. IV A are local in energy. Since in practice the final states are spread over a wide range of energies, we expect that the smooth envelope of the spectrum will vary with energy. The fluctuations that we should consider are with respect to this smooth envelope. It is, therefore, important to scale the intensity variations by their secular, smooth variation. This is accomplished by using Gaussians of width γ (to be chosen properly) centered around each level E_i

$$\bar{y}(E,E') = \frac{\sum_{i,f} |\langle f|T|i \rangle|^2 e^{-(E-E_i)^2/2\gamma^2} e^{-(E'-E_f)^2/2\gamma^2}}{\sum_{i,f} e^{-(E-E_i)^2/2\gamma^2} e^{-(E'-E_f)^2/2\gamma^2}} . \tag{48}$$

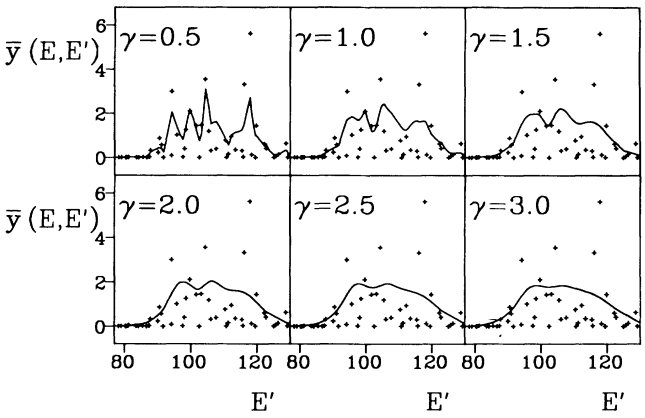

FIG. 7. The averaged $E2$ intensity $\bar{y}(E,E')$ for a transition between energies E and E' [Eq. (48)], plotted vs E' for $E=E_i$ ($i=100$th state) and for various values of γ.

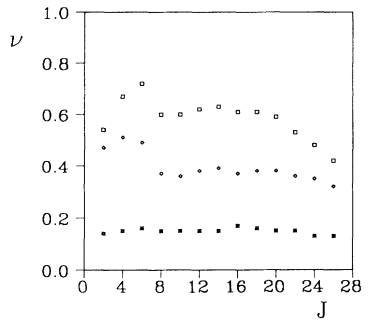

FIG. 8. ν vs spin J for $\chi=-1.05$ (diamonds), -0.5 (squares), and -0.01 (asterisks). Notice the decrease in ν (for $\chi=-0.5$) at high spins ($J\geq 20\hbar$).

We then renormalize the intensities y by dividing out their smooth part

$$y_{fi}\equiv|\langle f|T|i\rangle|^2/\bar{y}(E=E_i,E'=E_f)\ . \tag{49}$$

The statistics is then done on the y's defined by (49). It is important to choose γ properly. γ should be large enough so that the fine structure of the intensities will not show up. Yet it should not be too large so as to wash away the secular energy variations of the average intensity.

In the analysis of low-lying collective states of nuclei, $E2$ transitions play an important role. We have chosen $T(E2)$ to be the operator given by Eq. (4), and the intensities y are then the corresponding $B(E2)$ values

$$y\equiv B(E2;i\rightarrow f)=\frac{1}{2J_i+1}|\langle f\|T(E2)\|i\rangle|^2\ . \tag{50}$$

We have analyzed $E2$ transitions within a given spin/parity class as well as between different spin/parity classes.

In order to use a constant γ in Eq. (48), it is important to first find the unfolded energy levels $\tilde{E}_i$ (which have a constant mean spacing) and use them in Eqs. (48) and (49). To choose γ, we calculated $\bar{y}(E,E')$ for various γ's. An example is shown in Fig. 7 for the $E2$ transitions $8^+\rightarrow 8^+$ ($N=25$ and $\chi=-0.5$). The solid lines are

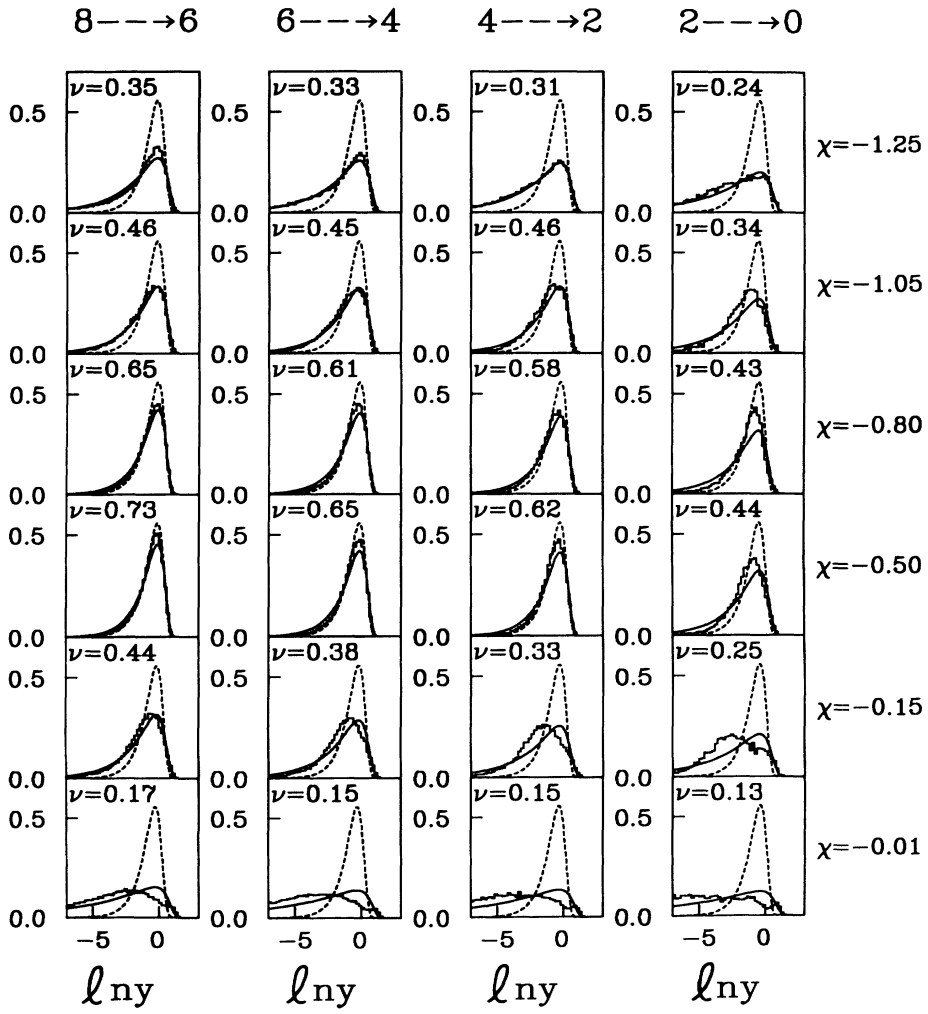

FIG. 9. The $E2$ intensity distribution vs ln$y$ for the transitions between states with different spins ($J\rightarrow J-2$). The dashed lines are the Porter-Thomas distribution and the solid lines are the fit to a χ^2 distributions with ν degrees of freedom.

$\bar{y}(E,E')$ versus E' for a fixed value of E given by $E=\tilde{E}_i$ (where $i=100$th state). The + symbols denote $|y_{fi}|^2$ for the same initial $|i\rangle$ state and various states $|f\rangle$. We see that for $\gamma=0.5$ and $\gamma=1$ $y(E,E')$ is not smooth enough. Reasonable values for γ are $1.5\lesssim\gamma\lesssim2.5$. We have chosen $\gamma=2$.

C. $B(E2)$ fluctuations versus χ and spin

Using the eigenstates of the Hamiltonian (1) and the $E2$ transition operator (4) we have calculated the $J^\pi\rightarrow J^\pi$ $B(E2)$'s. We renormalized them according to the method of Sec. IV B using $\gamma=2$, and histogrammed them into 20 bins, equally spaced in $\ln y$. The left-hand column of Fig. 2 shows examples of these distributions $P(y)$ for the $6^+\rightarrow6^+$ transition ($N=25$) and various values of χ. The dashed lines are Porter-Thomas distributions (31) with the same $\langle y\rangle$ as the actual $P(y)$ distributions. The solid line is the fitted distribution $P_\nu(y)$ with ν determined as explained in Sec. IV A. We see that near the regular limits ($\chi=-\sqrt{7}/2$ and $\chi=0$) the values of ν are the smallest. However, in the intermediate region the value of ν increases towards the GOE value of 1. This is consistent with the classical calculations that suggest the onset of chaos for intermediate values of χ. The maximal value of ν (in the above example) is $\nu\approx0.7$ for $\chi\approx-0.6$. This suggests that for the most "chaotic" value of χ, we have not reached complete chaos. The classical analysis does show that the onset of chaos is also energy dependent and that certain energy regions continue to stay regular even for $x\approx-0.6$. The intensity fluctuations correlate well also with the spectral fluctuations as seen from Fig. 2.

The spin dependence of ν is shown in Fig. 8 for several values of χ (-1.05, -0.5, and -0.01). In the chaotic region ($\chi=-0.5$) we see a significant drop in the value of ν at high spins. This agrees with our conclusion from Sec. III D that the degree of chaos is reduced at high spins.

D. $E2$ transitions between states with different spin

It is also interesting to analyze the statistics of the $E2$ transitions between states with different spins. These in-

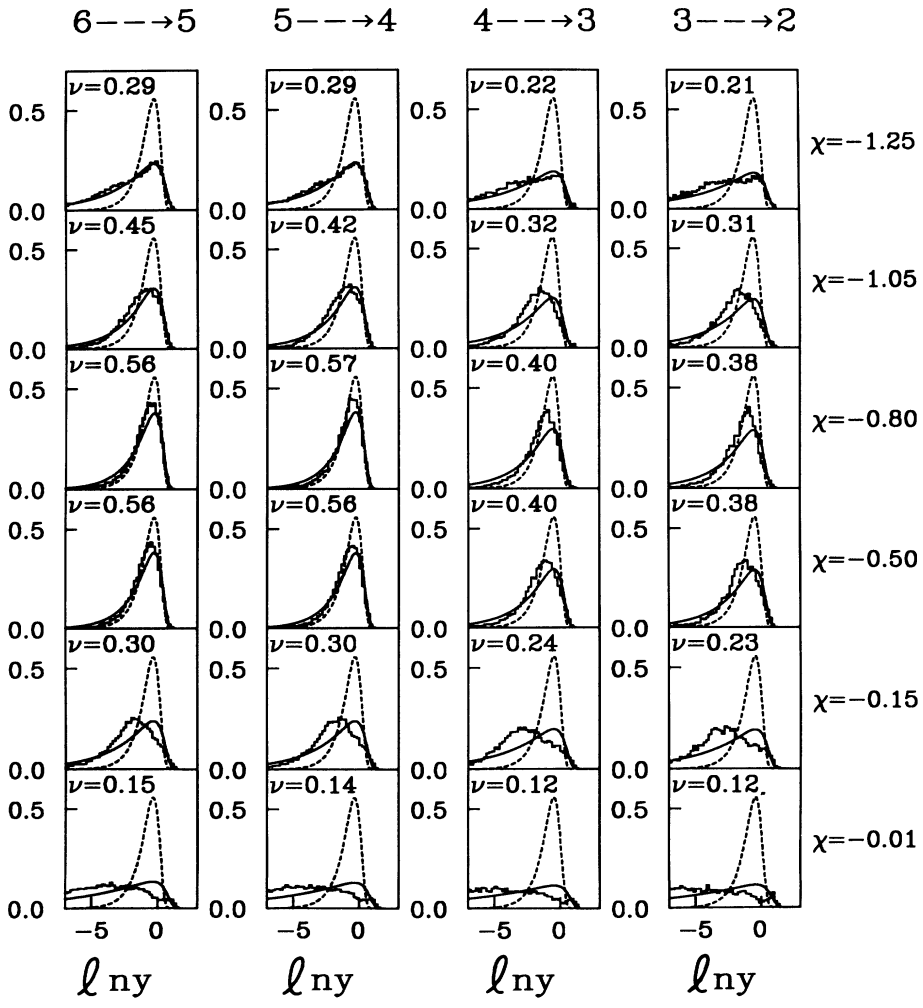

FIG. 10. As in Fig. 9 but for the $E2$ transitions $J\rightarrow J-1$.

clude transitions that occur within the same rotational band and in between different bands. Figures 9 and 10 show $E2$ distributions for transitions of the type $J \to J-2$ and $J \to J-1$, respectively. Their dependence on χ is consistent with all of our previous results: ν is small near the integrable limits ($\chi=-\sqrt{7}/2$ and $\chi=0$) and is closest to the Porter-Thomas value in the intermediate regime ($\chi \approx -0.8$ to -0.5). For a given χ, ν gets larger as the spin J increases (for low spins $J \lesssim 8\hbar$). Also the transitions $J \to J-1$ are less regular (i.e., have larger ν) than the transitions $J \to J-2$.

V. FINITE N EFFECTS

The results of the quantal statistics discussed in the previous sections correlate well with the classical analysis. There are, however, several finite N effects. At low spin ($J \lesssim 10$) we observe a staggering effect between even and odd spins (excluding $J=3$) where the even spins are somewhat more chaotic than the odd spins (see, for example, $\chi=-0.8$ and -0.5). This effect is easier to see in ν, for which the statistical error is much smaller than the corresponding one for ω. For example at $\chi=-0.8$, $\nu=0.68$ and 0.72 for $J=4$ and 6, respectively, while $\nu=0.52$ and 0.59 for $J=5$ and 7, respectively. For higher spins this quantal effect quickly disappears.

Another peculiar quantal effect is seen for the $J=0$ and $J=3$ (Fig. 11) statistics. Near the SU(3) limit ($\chi=-1.25$) they are much less regular ($\omega=0.5$ and 0.65 for $J=0$ and 3, respectively) than is the case for other spins. To explain this effect, note that at the SU(3) limit ($\chi=-\sqrt{7}/2$) for $J=0$ and 3 states there are no states with different K's that belong to the same SU(3) representation. For other values of J such states exist and are degenerate, therefore causing a stronger regularity near the SU(3) limit. For $J \neq 0$ the only allowed $E2$ transition in the SU(3) limit are those that do not change the SU(3) representation. Since for $J=3$ only one value of K exists in each SU(3) representation, only the diagonal $3^+ \to 3^+$ elements do not vanish. Thus near the SU(3) limit, there are not enough strong $3^+ \to 3^+$ transitions to have a significant decrease of ν from the GOE value.

Another interesting quantal effect is the saturation of the Δ_3 statistics, namely the flattening out of the Δ_3 curve at some nonuniversal finite L. This effect was explained semiclassically by Berry [11] using the level density expansion of Gutzwiller [34] and Balian and Bloch [35]. According to this expansion, the zero length classical trajectories contribute to $\rho_{\rm av}(E)$, while the fluctuating part of the level density is a sum over contributions from finite periodic trajectories each contributing a phase of $\exp[iS(E)/\hbar]$ with $S(E)$ the classical action along the respective trajectory. For a given L, the periodic orbits that contribute to $\Delta_3(L)$ are the ones whose action changes over the length L. They have a period $T \gtrsim \hbar\rho_{\rm av}/L$. As L increases above the value $L_{\rm max}$

$$L_{\rm max}=\hbar\rho_{\rm av}/T_{\rm min} , \tag{51}$$

where $T_{\rm min}$ is the shortest period, all trajectories contribute and $\Delta_3(L)$ will saturate.

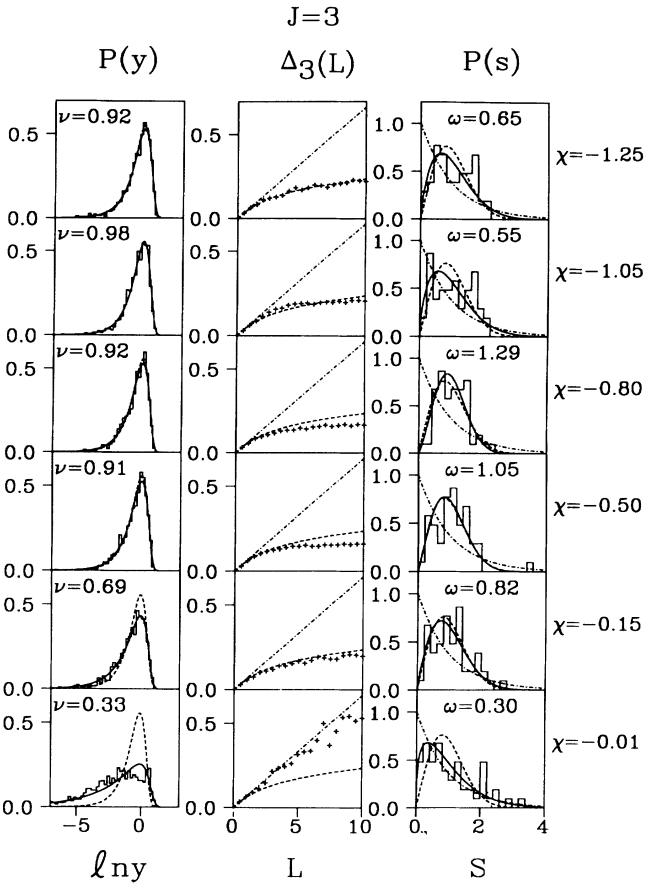

FIG. 11. The spectral and $E2$ intensity statistics for $J=3^+$ states. See Fig. 2 for details.

To find how $L_{\rm max}$ scales with the boson number N, we need to know the dependence of $\hbar$ and $\rho_{\rm av}$ on N. To find $\hbar$ we estimate the number of states for a system in five degrees of freedom by

$$\frac{V}{(2\pi\hbar)^5}=\frac{1}{1200\hbar^5} , \tag{52}$$

where $V=2\pi^5/10\Gamma(5)$ is the volume of the unit sphere in ten dimensions. Since the number of states in the quantal model is $\approx N^5/120$, we obtain

$$\hbar=\frac{10^{-1/5}}{N}\approx\frac{0.63}{N} . \tag{53}$$

$\rho_{\rm av}$ is the average density of states for given values of the angular momentum and its projection. Since $\rho_{\rm av} \propto N^3$, we obtain

$$L_{\rm max} \propto N^2/T_{\rm min} . \tag{54}$$

Thus the saturation length scales as N^2.

VI. CONCLUSIONS

We have studied the onset of quantum chaos in the low-lying collective states in nuclei, using the interacting

boson model. Both spectral and $E2$ intensity fluctuations were analyzed, and chaos was observed in the transition region between rotational and γ-unstable nuclei. The results are consistent with the classical analysis performed elsewhere [24]. The connection between quantum and classical chaos is confirmed in systems with more than two degrees of freedom.

ACKNOWLEDGMENTS

This work was supported in part by Department of Energy Contract No. DE-FG-0291-ER-40608. One of us (A.N.) acknowledges the hospitality of the Center for Theoretical Physics at Yale University. We thank N. Whelan for useful discussions.

[1] M. L. Metha, *Random Matrices* (Academic, New York, 1967).
[2] C. E. Porter, *Statistical Theories of Spectra: Fluctuations* (Academic, New York, 1965).
[3] T. A. Brody, J. Flores, J. B. French, P. A. Mello, A. Pandey, and S. S. M. Wong, Rev. Mod. Phys. **53**, 385 (1981).
[4] O. Bohigas, M. J. Giannoni, and C. Schmit, Phys. Rev. Lett. **52**, 1 (1984).
[5] T. H. Seligman, J. J. M. Verbaarschot, and M. R. Zirnbauer, Phys. Rev. Lett. **53**, 215 (1984); J. Phys. A **18**, 2715 (1985).
[6] G. Casati, B. V. Chirikov, and I. Guarneri, Phys. Rev. Lett. **54**, 1350 (1985).
[7] *Chaotic Behavior in Quantum Systems: Theory and Applications,* Vol. 120 of *NATO Advanced Study Institute, Series B: Physics,* edited by G. Casati (Plenum, New York, 1985).
[8] Th. Zimmermann, L. S. Cederbaum, H.-D. Meyer, and H. Köppel, J. Chem. Phys. **91**, 4446 (1987).
[9] D. C. Meredith, S. E. Koonin, and M. R. Zirnbaur, Phys. Rev. A **37**, 3499 (1988).
[10] J. C. Gay and D. Delande, Phys. Rev. Lett. **57**, 2879 (1986).
[11] M. V. Berry, Proc. R. Soc. London Ser. A **100**, 229 (1985).
[12] E. B. Stechel and E. J. Heller, Annu. Rev. Phys. Chem. **35**, 563 (1984).
[13] Y. Alhassid and R. D. Levine, Phys. Rev. Lett. **57**, 2879 (1986).
[14] Y. Alhassid and M. Feingold, Phys. Rev. A **34**, 374 (1989).
[15] R. V. Itag, A. Pandey, and O. Bohigas, Phys. Rev. Lett. **48**, 1086 (1982).
[16] Y. A. Abul-Magd and H. A. Weidenmüller, Phys. Lett. **162B**, 223 (1985).
[17] T. von Egidy, A. N. Behkami, and H. H. Schmidt, Nucl. Phys. **A481**, 189 (1988); J. F. Shriner, G. E. Mitchell, and T. von Egidy, Phys. Rev. C **43**, (1991).
[18] S. Raman *et al.*, Phys. Rev. C **43**, 521 (1991).
[19] J. D. Garrett, J. R. German, L. Courtney, and J. M. Espino (unpublished).
[20] Y. Alhassid, A. Novoselsky, and N. Whelan, Phys. Rev. Lett. **65**, 2971 (1990).
[21] H. Friedrich and D. Wintgen, Phys. Rep. **183**, 37 (1989).
[22] F. Iachello and A. Arima, *The Interacting Boson Model* (Cambridge University, Cambridge, England, 1987).
[23] A. Arima and F. Iachello, Ann. Phys. (N.Y.) **99**, 253 (1976); **111**, 201 (1978); **123**, 468 (1979).
[24] Y. Alhassid and N. Whelan, Phys. Rev. C **43**, 2637 (1991).
[25] W. Zhang, C. C. Martens, D. H. Feng, and J. Yuan, Phys. Rev. Lett. **61**, 2167 (1988).
[26] D. D. Warner and R. F. Casten, Phys. Rev. Lett. **48**, 1385 (1982); Phys. Rev. C **28**, 1798 (1983).
[27] *Dynamical Groups and Spectrum Generating Algebras,* edited by A. Bohm, Y. Ne'eman, and A. O. Barut (World Scientific, Singapore, 1988).
[28] G. Draayer and R. Gilmore, J. Math. Phys. **26**, 3053 (1985).
[29] O. Bohigas and M. J. Giannoni, in *Mathematical and Computational Methods in Nuclear Physics,* edited by J. S. Dehesa, J. M. Gomez, and A. Polls (Springer-Verlag, Berlin, 1983).
[30] H. Wu, D. H. Feng, and M. Vallieres, J. Phys. G **16**, L149 (1990).
[31] C. E. Porter and R. G. Thomas, Phys. Rev. 104, **483** (1956).
[32] *The Maximum Entropy Formalism,* edited by R. D. Levine and M. Tribus (MIT, Cambridge, MA, 1979).
[33] Y. Alhassid, N. Agmon, and R. D. Levine, Chem. Phys. Lett. **53**, 22 (1978).
[34] C. Gutzwiller, J. Math. Phys. **11**, 1791 (1970).
[35] R. Balian and C. Bloch, Ann. Phys. (N.Y.) **85**, 514 (1974).